Long-term change in the source contribution to surface ozone over Japan

Tatsuya Nagashima[1], Kengo Sudo[2,3], Hajime Akimoto[1], Junichi Kurokawa[4], and Toshimasa Ohara[1]

[1]National Institute for Environmental Studies, Tsukuba, Japan

[2]Graduate School of Environmental Studies, Nagoya University, Nagoya, Japan

[3]Frontier Research Center for Global Change, Yokohama, Japan

[4]Asia Center for Air Pollution Research, Niigata, Japan

Correspondence to: T. Nagashima (nagashima.tatsuya@nies.go.jp)

Abstract

The relative contributions of various source regions to the long-term (1980–2005) increasing trend in surface ozone (O_3) over Japan were estimated by a series of tracer-tagging simulations using a global chemical transport model. The model well simulated the observed increasing trend of surface O_3 including its seasonal variation and geographical features in Japan and demonstrated the relative roles of different source regions in forming this trend. Most of the simulated increasing trend of surface O_3 over Japan (~97 %) was explained as the sum of trends in contributions of different regions to photochemical O_3 production. The increasing trend in O_3 produced in China accounted for 36 % of the total increasing trend and those in the other northeast Asian regions (the Korean Peninsula, coastal regions in East Asia, and Japan) each accounted for about 12–15 %. Furthermore, the contributions of O_3 created in the entire free troposphere and in West, South, and Southeast Asian regions also increased; and their increasing trends accounted for 16 and 7 % of the total trend, respectively. The impact of interannual variations in climate, in methane concentration, and in emission of O_3 precursors from different source regions on the relative contributions of O_3 created in each region estimated above was also investigated. The variation of climate and the increase in methane concentration together caused the increase of photochemical O_3 production in several regions, and represented about 19 % of the total increasing trend of surface O_3 over Japan. The increase in emission of O_3 precursors in China caused an increase of photochemical O_3 production not only in China itself but also in the other northeast Asian regions and accounted for about 46 % of the total increase in surface O_3 over Japan. Similarly, the relative impact of O_3 precursor emission changes in the Korean Peninsula and Japan were estimated as about 16 and 4 % of the total increasing trend, respectively. The O_3 precursor emission change in regions other than northeast Asia caused increases in surface O_3 over Japan mainly through increasing photochemical O_3 production in West, South, and Southeast Asia and the free troposphere, and accounted for about 16 % of the total.

1 Introduction

Tropospheric ozone (O_3) is an oxidant and photodissociates to generate the hydroxyl radical which strongly oxidizes many atmospheric compounds including various air pollutants and thus removes them from the atmosphere. In contrast, high levels of O_3 are a major air pollutant due to adverse effects on human health, natural vegetation, and agricultural produce (Wang and Mauzerall, 2004; Mauzerall et al., 2005; US EPA, 2006; Silva et al., 2013). Moreover, tropospheric O_3 is a major greenhouse gas in the atmosphere, and reduction of its amount was recently recognized as an effective measure to mitigate near-term climate change (UNEP and WMO, 2011; Shindell et al., 2012). Therefore, the spatial and temporal variations in tropospheric O_3 have been always a matter of scientific and public concern.

Japan experienced a rapid industrialization ahead of other Asian countries, and an increasing trend has been found in various observations of O_3 over the past approximately 40 years. Routine ozonesonde measurements since 1970 at three Japanese sites of Sapporo (43° N), Tsukuba (36° N), and Kagoshima (32° N) showed an increasing trend of O_3 concentration in the lowermost troposphere up to about 1990 and relatively stable thereafter, with largest increase near the ground and discernible about 300 hPa height and below (Logan et al., 1999; Oltmans et al., 2006). With an air mass classification method based on backward air trajectories, Naja and Akimoto (2004) showed that a significant amount of the air masses reaching these ozonesonde sites in Japan spend substantial time over polluted regions in East Asia. The O_3 levels in these regionally polluted air masses increased from the 1970s to the 1990s, mainly due to large increases in nitrogen oxide (NO_x = NO + NO_2) emissions over China in the 1990s. Oltmans et al. (2013) analyzed a rather short period of data (1991–2010) obtained at the Ryori (39° N) surface site in north-eastern Japan and showed an increase into the mid-1990s followed by relatively little change. Other ground-based observations at a mountain site (Mt. Happo; 43° N, 1850 m asl) and three sites in the marine boundary layer along the west coast of Japan [Rishiri (45° N), Tappi (41° N), and Sado (38° N)], where few sources of pollutants exist nearby, obtained under the monitoring network of EANET (the Acid Deposition Monitoring Network in East Asia) also showed increasing trends of O_3 concentrations at least until the mid-2000s (Tanimoto, 2009; Tanimoto et al., 2009; Parrish et al., 2012). During the recent decades, an increasing trend in tropospheric O_3 has also been observed at many locations in East Asia including Taiwan (Chou et al., 2006; Chang and Lee; 2007; Li et al., 2010; Lin et al., 2010), mainland China (Lu and Wang, 2006; Ding et al., 2008; Xu et al., 2008; Wang et al., 2009; Zhang et al., 2014), and South Korea (Susaya et al., 2013; Lee et al., 2014; Seo et al., 2014). The increase rates of O_3 in those East Asian regions significantly vary depending on location and season in the range of about 0.3–3 ppbv/yr; however, the increases are generally larger than the trends in tropospheric O_3 for other regions in the world (Cooper et al., 2014).

In Japan, analysis of long-term observations by the ambient air quality monitoring network mainly established in urban–suburban regions also showed continuous increases of surface O_3 from the mid-1980s until the present (Ohara and Sakata, 2003; Ohara et al., 2008; Kurokawa et al., 2009; MOE Japan, 2013; Wakamatsu et al., 2013; Akimoto et al., 2015). And the consequent high violation rate of national ambient air quality standard (AAQS) for surface O_3 (hourly mean concentration of 60 ppbv) has been the persistent issue in environmental administration for a long time, therefore, there is an urgent need to study the reason for the increasing trend and examine the countermeasures. One clue is that the simultaneous observations of O_3 precursors such as NO_x and non-methane hydrocarbons (NMHCs) by this monitoring network revealed their decreasing trends in the same period (MOE Japan, 2013), which seemed inconsistent with the increasing trend of O_3 over Japan. These observed

features of O_3-related atmospheric species in Japan suggest that there should be an influence of transboundary transport from outside of Japan on the recent increasing trend in O_3. The influence of transboundary transport on surface O_3 in East Asia was examined in several studies (Sudo and Akimoto, 2007; Li et al., 2008; Nagashima et al., 2010; Wang et al., 2011). Nagashima et al. (2010) demonstrated that the O_3 transported from outside of Japan accounted for more than 70 % of surface O_3 over Japan in the cold season (October–March) during 2000–2005, and most was attributable to O_3 from distant sources outside East Asia and from the stratosphere. In the warm season (April–September), the contribution of domestically created O_3 in Japan to surface O_3 over Japan increased significantly (about 20–40 %), the short range intra-regional transport of O_3 from other parts of East Asia still contributed about 25 %, and long range inter-regional transport of O_3 from outside East Asia and the stratosphere particularly in spring could account for about half of surface O_3 over Japan.

Therefore, the influence of O_3 from source regions outside and inside East Asia and the stratosphere should be considered to explain the cause of the increasing trend in surface O_3 over Japan. The rapid increase in O_3 precursor emissions in East Asia in recent decades (Ohara et al., 2007; Kurokawa et al., 2013) was demonstrated as a major cause of the increasing trend of springtime O_3 over Japan by comparing regional chemical transport model (CTM) simulations of recent decades with and without the East Asian O_3 precursor emission increases during the period (Kurokawa et al., 2009; Tanimoto et al., 2009). However, they only showed the springtime O_3 case and it was unclear whether the relationship held in other seasons. Moreover, the relative contributions of individual countries or regions in East Asia have not been well examined, particularly concerning increased surface O_3 over Japan.

Here, we investigated the cause of the continuous increase in surface O_3 over Japan reported in the above literature, focusing on the relative contributions of various source regions over the globe, particularly the contributions of individual regions in East Asia, with a long-term simulation of a global CTM using the tagged tracer method. Using the same model and method, Nagashima et al. (2010) showed such relative contributions of regions inside and outside East Asia on surface O_3 over Japan as average values for the early 2000s. The current study investigated the temporal evolution of the relative contributions of each region for the 26 years of 1980–2005.

2 Methods

2.1 Model description

In this study, we employed a chemistry climate model (CCM), CHASER (Sudo et al., 2002), developed for the atmospheric chemistry research in the troposphere. The basic setting of the model was almost identical to that used by Nagashima et al. (2010). However, the horizontal resolution was modified from T63 (about 1.9° by 1.9° grid spacing in longitude and latitude) to T42 (about 2.8° by 2.8°), because longer simulation period was necessary than in the previous study, and so the cost of computation was reduced in the present study by selecting lower horizontal resolution. There were 32 vertical layers with the top layer set at approximately 40 km altitude. A detailed tropospheric photochemistry consisted of 113 chemical reactions and 27 photodissociation involving O_3, HO_x, NO_x, methane (CH_4), CO and NMHCs calculated the temporal evolution in the concentrations of 53 chemical species. The concentrations of O_3 and some nitrogen compounds (NO_x, HNO_3, and N_2O_5) above the tropopause that should affect tropospheric chemistry were assimilated into the monthly mean output data of stratospheric CCM, because the version of CHASER used was unable to

calculate several chemical processes, such as halogen-related chemical reactions, which are indispensable for realistic representation of such chemical compounds in the stratosphere. The model also included dry and wet deposition of chemical species.

In this study, we conducted tracer-tagging simulation by using two different setups (full-chemistry and tracer-transport setups) of CHASER. The full-chemistry setup calculated the actual temporal change in the concentration of chemical species through the abovementioned chemical and physical processes and outputted the chemical production and loss tendencies of O_3 and related species. Then, the tracer-transport setup used the outputted chemical tendencies to calculate the temporal change in the concentration of hypothetical O_3 tracers. In the following subsection, the calculation procedure is briefly described.

2.2 Outline of the numerical simulations

2.2.1 Forcings for long-term simulation

Long-term simulation was performed for the period 1980–2005. The end of simulation period (2005) was determined mainly due to the temporal coverage of the Asian emission data described below, however, this period sufficiently covered the years reported to have increasing trend in surface O_3 over Japan in the previous literatures. To drive the physical properties of the model for this 26-year period, the temperature and horizontal wind velocities in the model were assimilated into the National Center for Environmental Prediction/National Center of Atmospheric Research (NCEP/NCAR) 6-hour reanalysis data (Kalnay et al., 1996) of the corresponding year, and sea surface temperature and sea ice data of the Hadley Centre's Sea Ice and Sea Surface Temperature (HadISST) data set (Rayner et al., 2003) were used in the model.

The monthly mean stratospheric O_3 data of Akiyoshi et al. (2009) was used for the assimilation above the tropopause for this period. These data were the output of a stratospheric CCM simulation according to the hindcasting scenario for 1980–2004 (REF1 scenario) of the CCM validation activity (CCMVal) (Eyring et al., 2005), and included an interannual variation (IAV) associated with the 11-year solar cycle and large declines after 1982 and 1991 due to the El Chichon and Pinatubo eruptions, respectively, in addition to a continuous decreasing trend during the whole period. Although the simulated declines of stratospheric O_3 due to the two large volcanic eruptions were somewhat overestimated, the simulated IAVs in stratospheric O_3 reasonably well represented those observed with a total ozone mapping spectrometer (TOMS) from satellites (Akiyoshi et al., 2009). Incidentally, the stratospheric O_3 data of 2004 were used for 2005.

The long-term variation of the emissions of O_3 precursors (NO_x, CO, and NMHCs) were taken from multiple emission inventories. For anthropogenic emissions in Asia, the Regional Emission inventory in ASia (REAS ver.1.2) (Ohara et al., 2007) was used for each year in the whole simulation period (1980–2005). Kurokawa et al. (2009) used these emission data with a regional air quality model representing well the interannual variability of surface O_3 over Japan for similar period (1981–2005) to the present study. For anthropogenic emissions outside Asia, a combination of three versions of EDGAR (Emission Database for Global Atmospheric Research) emission data was used: EDGAR-HYDE (Van Aardenne et al., 2001) for 1980 and 1990; EDGAR v3.2 (Olivier and Berdowski, 2001) for 1990 and 1995; and EDGAR v3.2 Fast Track 2000 (FT2000) (Olivier and Berdowski, 2001) for 2000. Because several emission sectors considered in EDGAR v3.2 were not considered in EDGAR-HYDE,

the emissions for 1990 in EDGAR-HYDE were generally smaller than in EDGAR v3.2. Therefore, we used EDGAR v3.2 data for 1990, and also scaled them to estimate emission data for 1980 rather than simply using EDGAR-HYDE data for 1980. For that, we scaled EDGAR v3.2 data for 1990 so that the ratio (r) of the difference between 1980 (f_1) and 1990 data (f_2) and their average in EDGAR-HYDE [i.e., $r = (f_2 - f_1)/(f_1 + f_2)/2$] equaled the corresponding ratio (R) calculated from 1990 data in EDGAR v3.2 (F_2) and 1980 data scaled from it (F_1) [i.e., $R = (F_2 - F_1)/(F_1 + F_2)/2$]. We calculated F_1 from the known values of f_1, f_2, and F_2 using the equation $r = R$. Since EDGAR emission data were not available for each year but for every 10 or 5 years in the simulation period, the emissions for intermediate years were interpolated, and FT2000 data used for years after 2000. The vegetation fire emission data developed in the REanalysis of the TROpospheric chemical composition over the past 40 years project (RETRO) (Schultz et al., 2008) were used for O_3 precursor emissions from biomass burning for each year until 2000 in the simulation period, and data for 2000 were used for years after 2000. Historical transition of the atmospheric concentrations of carbon dioxide, nitrous oxide, and CH_4 were prescribed with those used in Nozawa et al. (2005), which were somewhat old estimations of the historical evolution in greenhouse gas concentrations, but not much different from recent estimations such as for the Representative Concentration Pathways (RCPs) (Meinshausen et al., 2011). The difference in the concentrations between both estimations were generally within a couple of percent in the simulation period.

The linear trends of NO_x and NMVOC annual emissions used in this study in the simulation period of 1980–2005 are shown in Fig. 1. The long-term trends of emissions of both species showed generally similar geographical features to each other; large decrease trends in central Europe, Scandinavia, western Russia, and Kazakhstan, whereas there were widely spread increasing emissions in West, South, Southeast, and East Asia, almost all Africa and Central and South America except for inland Brazil. In North America, NO_x emission generally decreased in the simulation period except for the west coast and New England area of the USA, but that of NMVOC mostly increased with a few patchy exceptions. The trends of NO_x and NMVOC emissions mentioned above were mainly due to the change in anthropogenic emissions, while the change in biomass burning emissions led to a discernible trend in several regions such as inland Brazil and the south of Sahel.

The long-term evolution of annual emissions of NO_x and NMVOC over several source areas in the Northern Hemisphere is shown in Fig. 2. Because the emission data were the combination of three different datasets outside Asia, there were somewhat discontinuous changes at the joint years (1990 and 1995) in European and North American emissions. The emissions of NO_x and NMVOC over Europe had peaks around 1990 and generally decreased afterward. Over North America, both species showed small long-term trends: slight decreases in NO_x and slight increases in NMVOC emissions. The emissions of both species over China greatly increased during the whole period. The NO_x emissions were about 4.0 times larger in 2005 than 1980 and correspondingly NMVOC was 2.5 times larger, which made emissions of both species for China equal to or even surpassing those for Europe or North America in 2005. The emissions of both species over the Korean Peninsula increased approximately 2.8 times during this period. However, those over Japan showed no such increase: NO_x emission decreased until 1995 and thereafter remained stable, whereas NMVOC emissions went up until 1995 and then slightly decreased.

2.2.2 Tracer tagging

We conducted a 26-year simulation using the full-chemistry setup of CHASER with all the forcings mentioned above, followed by another 26-year simulation with the tracer-transport setup of CHASER which calculated the concentration of hypothetical O_3 tracers, each tagged with a particular region in the model domain. The procedure to tag a tracer with each region in the second simulation was the same as used by Nagashima et al. (2010) and a brief description follows. In the second simulation, the transport and dry deposition of each O_3 tracer were calculated same as in the first simulation, however the chemical development of tracers was calculated using the chemical production (P) and loss frequencies (L) of the extended odd oxygen family [$O_x = O_3 + O + O(^1D) + NO_2 + 2NO_3 + 3N_2O_5 + PANs + HNO_3$ + other nitrates] calculated and archived in the first simulation. In the first simulation, 3D fields of P and L were outputted every 6 hours. Each O_3 tracer could be lost chemically everywhere in the model domain at the frequency of L, but could be chemically produced only inside its tagged region. In the stratosphere, the concentration of O_3 tracer tagged with the stratosphere was assimilated into the same stratospheric O_3 data as used in the first simulation, but the concentration of the tracers tagged with the region in the troposphere were all set to zero. The calculated concentration of each tagged O_3 tracer at a given location represents the contribution of O_3 produced in each source region and transported to that location.

The troposphere in the model domain was horizontally separated into 22 regions and each horizontal region was further separated vertically between the free troposphere (FT) and the planetary boundary layer (PBL). The stratosphere was considered one separate source region, that is, the model domain was separated into 45 source regions. The 22 regions for horizontal separation are shown in Fig. 1 and each region was assigned a three-letter code (e.g., AMN for North America) which is used in the following sections. For the vertical separation of the source regions in the troposphere, the PBL was defined as the lowest six layers in the model (surface to about 750 hPa), based on the observed and modeled vertical profiles of O_3 production.

The long-term tracer-tagging simulation allowed estimation of the long-term variations in contributions of each source region to the O_3 concentration at given receptor locations. This is important information to explain the cause of the reported increasing trend in surface O_3 over East Asia. However, it should be noted that the tracer-tagging simulation calculates the amount of O_3 in a receptor location that was produced chemically in each source region from O_3 precursors emitted both from the source region and adjacent source regions. Thus, the contribution of a source region estimated in tracer-tagging simulation should not be fully attributed to emissions of O_3 precursors in that source region. Emission sensitivity simulation is another method of estimating the portion of O_3 fully attributable to a change in O_3 precursor emissions in a source region, and takes the difference of simulated O_3 between two model runs with and without perturbed O_3 precursor emissions in that source region. The resulting estimations of source contributions by the two methods can differ; however, the differences have not yet been well quantified. Li et al. (2008) reported that the difference between the two methods could be as much as 30 % in source apportionment estimation for one location and time (i.e., Mt. Tai in central eastern China in June 2006). Wang et al. (2011) found somewhat larger differences in the contributions of China to domestic O_3 concentration between the two methods for each month of the year, but no discussions were made for O_3 over Japan.

Nevertheless, we employed the tracer-tagging simulation to study the cause of reported long-term change in surface O_3 over Japan mainly due to its computational efficiency. Thus, the

results should be carefully interpreted in terms of the difference between the source regions of chemical O_3 production and those of O_3 precursor emissions. The computational efficiency resulting from the tracer-tagging approach and relatively coarse horizontal resolution enabled us to make several sensitivity simulations with the different combination of forcings for long-term simulation. In the following sections, the simulation with the full set of long-term forcings described above, hereinafter referred to as "standard" simulation, is initially analyzed. This is then further interpreted using the results of sensitivity simulations; the specific settings of sensitivity simulations are also described.

3 Results and discussion

3.1 Long-term evolution of surface O_3 over Japan

Nagashima et al. (2010) validated how well CHASER can reproduce the observed features of surface O_3 concentrations by comparing the simulated surface O_3 concentrations with observations taken during 2000–2005 at several sites mainly in rural areas in the Northern Hemisphere, and CHASER successfully simulated the annual variation of surface O_3 in a variety of regions. In this study, the horizontal resolution of the model differed from that used in Nagashima et al. (2010); however, the model well represented the observed concentrations and seasonal evolutions of surface O_3 (Fig. S1 and Table S1 in the Supplement). The surface O_3 over Japan has been observed at ambient air quality monitoring stations since the early 1970s. The monitoring data have been compiled by the Atmospheric Environmental Regional Observation System (AEROS). About 1000 monitoring stations widely distributed throughout Japan except in the southern islands could be used for validation of the model results. The monitoring data of AEROS have been used to examine the long-term variation of surface O_3 over Japan in several studies and showed significant increasing trends (Ohara and Sakata, 2003; Ohara et al., 2008; Kurokawa et al., 2009; Akimoto et al., 2015). We validated the simulated surface O_3 over Japan with the AEROS data in terms of the long-term variation in the following.

For the validation, the monitoring sites selected had continuously observed the surface O_3 during the simulation period (1980–2005). To ensure continuity of sites, we selected monitoring sites with annual mean surface O_3 available for every year in the simulation period. The annual mean data at a monitoring site was calculated as the average of monthly means when available for more than 9 months, the monthly mean was calculated from daily means when available for over 19 days per month, and the daily mean was calculated from hourly means when available for more than 19 hours per day. There were 339 sites, located mainly in populated areas of Japan except in the northernmost island (Hokkaido) and southern islands (Nansei Islands). We first calculated the annual mean surface O_3, and then the annual means of all sites were averaged to calculate the observed annual mean surface O_3 over Japan. The simulated annual mean surface O_3 over Japan was calculated as the average of annual means of the model grids, which included the locations of monitoring sites selected for the validation. The temporal variations of observed and simulated annual mean surface O_3 anomalies during 1980–2005 averaged over Japan are shown in Fig. 3. During the period, the observed annual mean surface O_3 over Japan showed a clear increasing trend with a linear increase of about 2.70 ppbv/decade, which was significant at the 5 % risk level. The simulated annual mean surface O_3 over Japan also showed a significant increasing trend with a rate of about 2.58 ppbv/decade, which corresponded well to the observed increase in surface O_3 over Japan. The value of the linear increasing trend and the observed features of long-term variation in surface

O_3 over Japan – such as a rapid increase from the mid-1980s to the mid-1990s followed by a stagnation of increase for about 7–8 years and a further increase in the past several years – were reasonably well captured by the model.

The model also well represented the longitudinal differences in the long-term trend of surface O_3 in Japan. Figure 4 shows the maps of linear trends of annual mean surface O_3 during 1980–2005 calculated from the model simulations and observations at AEROS monitoring sites as selected for Fig. 3. The simulated annual mean surface O_3 showed an increasing trend in the whole area including all of Japan and the Korean Peninsula (Fig. 4a). The simulated increasing trend of annual mean surface O_3 well exceeded 2.0 ppbv/decade in wide areas of Japan except for Hokkaido, and tended to be greater toward western Japan, which is nearer to the Asian continent. However, the increasing trends of observed annual mean surface O_3 at each monitoring site (Fig. 4b) differed greatly from each other even in nearby sites, and there was no apparent longitudinal tendency in trends at individual monitoring sites. However, we averaged the observed annual mean surface O_3 at individual monitoring sites at longitudinal intervals (approximately 2.8°) of the model grids as shown by gray rectangles (Fig. 4b) and calculated the long-term trend of averaged monitoring data at each longitudinal band. The calculated increasing trends were clearly larger toward the west, which was consistent with westward rise of the increasing trends of simulated data.

There were seasonal differences in the long-term increasing trend of surface O_3 over Japan. The temporal variations of observed and simulated seasonal mean surface O_3 anomalies during 1980–2005 averaged over Japan are shown in Fig. 5. The increasing trend of surface O_3 over Japan in the monitoring data was greatest in spring (March–May: 4.04 ppbv/year) and was also large in summer (June–August: 3.07 ppbv/year); in contrast, increasing trends were relatively small in fall (September–November: 2.29 ppbv/year) and winter (December–February: 1.28 ppbv/year). Seasonal dependency in the increasing trends of observed surface O_3 over Japan has been previously reported (Ohara and Sakata, 2003; Parrish et al., 2012). Ohara and Sakata (2003) examined almost the same O_3 monitoring data in Japan as used in the present study for the period 1985–1999 and showed year-round increase in surface O_3 from 1985–1987 to 1997–1999 with a greater increase in the warm season (March–August) than in the rest of the year. Parrish et al. (2012) summarized long-term changes in lower tropospheric baseline O_3 over the world including two regions in Japan (Mt. Happo and several sites in the marine boundary layer grouped as one region), and showed that the increasing trend of surface O_3 was greatest in spring and least in fall in these two regions. In the present study, the simulated increasing trend in seasonal mean surface O_3 was also larger in the warm (spring–summer) than in the cold season (fall–winter), consistent with the observed increasing trends.

As described above, our model captured well the basic features of long-term trends in observed surface O_3 over Japan, which allowed us to use the simulated data for further analysis on the source of the long-term trend in the next section.

3.2 Contributions of O_3 production regions

The tracer-tagging simulation for 1980–2005 was conducted, and the IAVs in the annual mean concentrations of each tagged O_3 tracer averaged over Japan are shown in Fig. 6. The tagged tracers other than FT and stratosphere in Fig. 6 and the following figures represent the contribution of O_3 produced in the PBL of different source regions shown in Fig. 1, where contributions of several source regions were grouped into some combined source regions. It

should be noted that the model grids used for averaging in these figures differed from those in Figs. 3–5. They encompassed almost all of Japan excluding the Nansei Islands in order to examine temporal behavior of tagged O_3 tracers in all of Japan (see Fig. 4 for actual areas for averaging).

Domestically created O_3 was the largest contribution to surface O_3 concentration averaged over Japan during the whole simulation period. The contribution of domestic production had a large IAV and was larger in the last decade (1996−2005) than previously.

The second largest contribution was the O_3 created in the FT as a whole during almost the entire period. For the FT, the northern mid-latitude regions such as North Pacific (NPC), Europe (EUR), North Atlantic (NAT), North America (AMN), and China (CHN) made leading contributions during the period; however, the increasing trend of these contributions was considerable particularly for CHN and NPC (Fig. S2). Despite such differences among the regional contributions in the FT, we hereafter only considered the total of each regional contribution in the FT, since it was difficult to associate a regional contribution with a particular source region of O_3 precursor emissions. The precursors eventually resulted in O_3 production in a region in the FT can be transported longer distance due to faster wind speed in the FT and therefore would be influenced by emissions from a wider range of source regions than in the PBL. The total FT contribution showed an increasing trend during the period.

The NO_x emission from lightning was an indispensable source of NO_x in the FT. The global annual lightning-NO_x emission in the current simulation was about 3.1 TgN/year averaged over the entire period and showed a small but significant increase of about 0.012 TgN/year (0.39 %/year). The increase in lightning-NO_x emission was a consequence of changes in convection activities due to the change in climate forced into the model during the period. However, this increase in lightning-NO_x emission was not the main cause of the increase in the contribution of the total FT – because a sensitivity simulation with all emissions, CH_4 concentration, and stratospheric O_3 fixed at the year 1980 level but with the same temporal evolution in climate showed a quite similar increase in lightning-NO_x emission but no significant increasing trend in the total FT contribution. Therefore, the main cause of the increasing trend in the total FT contribution was likely to be factors other than the increase in lightning-NO_x emission.

The contribution of stratospheric O_3 was also large during the entire period, with considerable temporal fluctuations. The large decreases of stratospheric contribution in the early 1980s and 1990s stemmed from the decline of stratospheric O_3 concentration due to the impact of large volcanic eruptions of Mt. El Chichon in 1982 and Mt. Pinatubo in 1991, respectively (Akiyoshi et al., 2009).

In the early 1980s, the combined contributions of far remote regions from Japan in the northern mid-latitude (Remote: EUR, NAT, and AMN) made a significant contribution, the fourth largest, to the surface O_3 over Japan and remained at a steady level of contribution during the study period. At the same time, the contribution of CHN significantly increased from the mid-1980s, overtook the contribution of Remote in the early 1990s, and became the largest single regional contribution – excluding the domestic one (i.e., JPN). Moreover, the contributions of O_3 produced in the Korean Peninsula (KOR), the coastal regions in East Asia [E-Asia-Seas: NPC, East China Sea (ECS), and Japan Sea (JPS)], and West-South-SouthEast (WSSE) Asian regions [including Middle East (MES), India (IND), Indochina and Philippines (IDC), and Indonesia etc. (IDN)] also showed obvious increasing trends.

The linear trend (ppbv/decade) of annual mean tagged O_3 tracers during the simulation period as well as that of the total O_3, which is the sum of all tagged O_3 tracers averaged over

whole Japan (JPN-ALL) and those averaged over three sub-regions in Japan: western (JPN-W), eastern (JPN-E), and northern (JPN-N) Japan is shown in Fig. 7 (see Fig. 4 for the definition of sub-regions). The trend was calculated from the annual mean concentrations. The increasing trend of total O_3 averaged over JPN-ALL was 2.37 ppbv/decade, which was somewhat smaller than estimated in Fig. 3 (2.58 ppbv/decade) due to inclusion of model grids in JPN-N for averaging where the simulated increasing trend of O_3 was relatively small. The increasing trend of total O_3 tended to be greater westward. The absolute contribution of domestically produced O_3 in Japan differed among the regions – it tended to be larger in JPN-E than other parts of Japan (Nagashima et al., 2010); however, there were no such regional differences in long-term trends. The westward tendency of larger increasing trends in total O_3 over Japan was mainly due to the similar tendency in the trends of the contribution of CHN, KOR, and E-Asia-Seas, which strongly suggested a large impact of intra-regional transboundary air pollution in East Asia. In particular, the increasing trend in the CHN contribution was the largest for all sub-regions in Japan. The increasing trend in the contributions of total FT and WSSE Asia was slightly smaller for JPN-N than for other parts of Japan, which also contributed to the regional differences of the trend in total O_3 over Japan. Due to the large interannual fluctuation, the linear long-term trend of the stratospheric contribution was non-significant for all regions in Japan.

The linear trend of tagged O_3 tracers and total O_3 averaged over all of Japan in spring, summer, fall, and winter is shown in Fig. 8. The increasing trends of total O_3 in decreasing order were spring, summer, winter, and fall. This is quite consistent with the seasonal differences in the increasing trend of O_3 observed at several Japanese sites from the 1990s to 2011 (Parrish et al., 2012). The increasing trend in the CHN contribution was the largest of all contributions in all four seasons and the trend was particularly large in spring. The KOR contribution was also larger in spring than in other seasons. The contribution of E-Asia-Seas increased significantly in all seasons. Seasonal differences in the increasing trend in the E-Asia-Seas contribution were small, but were slightly larger in the warm (spring–summer) than the cold season (fall–winter). The increasing trend in domestic (JPN) contribution was larger in spring than in summer similarly to the cases of CHN and KOR contributions, but trends in both seasons were non-significant; whereas those in the cold season were significantly larger than in the warm season. The FT and WSSE Asian contributions showed semi-annual change in their increasing trends; larger in summer and winter than in spring and fall. The contribution of Remote showed a significant increasing trend only in winter. The seasonal features in each regional contribution described above enabled explanation of the cause of the seasonality of increasing trend in total O_3 over Japan as follows. The largest increasing trend of total O_3 in spring was predominantly attributed to the large increasing trend in contributions of source regions in northeast Asia (CHN, KOR, E-Asia-Seas, and JPN). The increasing trends in the contributions of CHN, KOR, and JPN were smaller in summer, however, partly compensated by the growth of increasing trends in the FT and WSSE Asian contributions from spring to summer. In the cold season, trends for most regions were smaller than in the warm season, except for JPN. The increasing trend in contributions of northeast Asian regions differed little between fall and winter; however, those of FT, WSSE Asia, and Remote had larger increasing trends in winter than in fall, which made the increasing trend of total O_3 in winter larger than in fall.

Table 1 summarizes the linear trends of annual mean tagged O_3 tracers and the total O_3 averaged over JPN-ALL. The vast majority (about 97 %) of the trend in total O_3 was balanced with the sum of those trends in regional contributions with statistical significance. The largest contribution was from the increase of O_3 produced in CHN (0.85 ppbv/decade), which

corresponded to about 36 % of the increasing trend of total O_3. The increasing trend in the contribution of the total FT was also large (0.37 ppbv/decade), representing about 16 % of the total O_3 trend. The contributions of northeast Asian regions other than CHN also increased significantly (0.34, 0.29, and 0.27 ppbv/decade for KOR, E-Asia-Seas, and JPN, respectively) and each accounted for about 12–15 % of the total O_3 trend. About 7 % of the total O_3 trend was attributable to the increasing trend in WSSE Asian contributions (0.16 ppbv/decade). The linear trends in the contributions of remaining regions were small and non-significant, and so were not important concerning the cause of reported surface O_3 increase over Japan.

3.3 Impact of temporal variations in O_3 precursor emissions in different source regions on regional O_3 production

The results in the preceding section revealed the relative importance of O_3 produced in different regions to the recent increasing trend in surface O_3 over Japan. It is noteworthy that this does not indicate the relative importance of the different regions of O_3 precursor emissions. For example, there were significant contributions of E-Asia-Seas to the increasing trend in surface O_3 over Japan, but there were clearly no large emission sources of precursors in these maritime regions other than navigation. The increasing trend in the contribution of E-Asia-Seas was likely a consequence of increased transport of O_3 precursors to this region, which had been emitted in adjacent land areas. However, the tracer-tagging approach cannot distinguish the differences in origins of emissions of precursors that resulted in O_3 production in E-Asia-Seas. To further investigate the roles of different regions in the recent increasing trend of surface O_3 over Japan, we performed a series of sensitivity simulations with different assumptions for the temporal variation of factors, which would affect the surface O_3 over Japan. Each sensitivity simulation consisted of a 26-year simulation with full-chemistry setup of CHASER followed by another 26-year simulation with tracer-tagging setup of CHASER. Initially, a sensitivity simulation was performed that was only forced by the IAVs in the climate but with all emissions of O_3 precursors, CH_4 concentration, and stratospheric O_3 fixed at the year 1980 level; then we gradually added the temporal variation of chemical factors as summarized in Table 2. The simulation F, driven by the temporal variation of all forcings, was identical to the standard simulation; and simulation A was mentioned concerning lightning-NO_x emission in the preceding section (3.2).

The linear trends of annual mean total O_3 and tagged O_3 tracers that had significant effects on the standard simulation averaged over all of Japan in all simulations are shown and compared in Fig. 9. Simulation A showed no obvious increasing trend in total O_3 over Japan. The surface temperature over Japan in the model which was assimilated into NCEP/NCAR reanalysis data showed a warming of 0.44 ± 0.21 °C/decade in the annual mean during the simulation period which well corresponded to the observed warming of 0.45 ± 0.23 °C/decade (JMA, 2017). The IAV of the surface temperature was well captured by the model too, although the modelled temperature was somewhat warmer than the observation in 2000s particularly in winter which might be related to the slight overestimation of winter surface O_3 in the model depicted in Fig.5. The JPN and total FT contributions exhibited increasing trends (0.12 and 0.06 ppbv/decade, respectively), likely due to the IAV of the climate, but they were non-significant.

The increase in atmospheric concentration of CH_4 was added in simulation B, because this would have a non-negligible impact on tropospheric O_3 (background O_3 in particular), as frequently reported (Brasseur et al., 2006; Kawase et al., 2011; HTAP, 2010 and references

therein). In the simulations other than A, we used a CH_4 concentration increase rate of about 12.3 ppbv/year (0.73 %/year) during 1980–2000 and flattened thereafter. In simulation B, the contribution of the total FT showed a significant increasing trend (0.18 ppbv/decade) as did that of Remote (0.08 ppbv/decade; data not shown). The contributions of several other regions such as CHN, E-Asia-Seas, and WSSE Asia also showed slight increasing trends (approximately 0.01–0.02 ppbv/decade), although non-significant. Note that these values included the impact of CH_4 increase as well as the IAV of the climate and, consequently, the total O_3 in simulation B showed a significant increasing trend of about 0.44 ppbv/decade, representing about 19 % of the increasing trend in total O_3 in the standard simulation (2.37 ppbv/decade).

In simulations C–E, the temporal variations in emission of O_3 precursors in northeast Asian regions were gradually added: CHN, KOR, and JPN, respectively. The increase in emissions of O_3 precursors in CHN in simulation C caused a large significant increasing trend in the contribution of CHN itself (0.83 ppbv/decade). Moreover, the emission increase in CHN also had a large impact on the contributions of other regions, in particular, the increase trends in the contributions of KOR and E-Asia-Seas became significant: 0.12 and 0.15 ppbv/decade, respectively. The JPN and the total FT contributions also showed somewhat larger increasing trends in simulation C than in B, but the growth in trends between the two simulations was not as large as those of KOR and E-Asia-Seas. The total effect of the emission increase in CHN on the increasing trend in surface O_3 over Japan, assessed using the difference in total O_3 trend between simulations B and C, was about 1.08 ppbv/decade and corresponded to about 46 % of the increasing trend in total O_3 in the standard simulation. The relative contribution of CHN as a source region of O_3 production to the surface O_3 increasing trend over Japan was estimated as 36 % in the preceding section (3.2); however, the contribution of CHN as a source region of O_3 precursors emission was somewhat (10 %) larger due to the production of O_3 outside CHN. It is noteworthy that the slight increasing trend in the contribution of WSSE Asia shown in the CH_4 increase in simulation B was smaller in simulation C. The contributions of Remote and the stratosphere showed similar responses. The increase in O_3 precursor emissions in CHN seemed to partly offset the increase in influence of long range transport of O_3 from such regions.

The increase in emissions from KOR in addition to CHN in simulation D gave rise to a much larger increasing trend in the contributions of KOR itself (0.38 ppbv/decade). Compared with simulation C (0.12 ppbv/decade), about one-third of the increasing trend in the contribution of KOR was attributed to the O_3 precursor emission increase in CHN and the rest to emission increase in KOR. Similarly, the emission increase in KOR caused a larger increasing trend in the contributions of E-Asia-Seas in simulation D (0.25 ppbv/decade). We attributed about half of the increasing trend in the contribution of E-Asia-Seas in the standard simulation (0.29 ppbv/decade) to the impact of O_3 precursor emission increase in CHN (and partly that of the CH_4 increase: 0.15 ppbv/decade) as shown in simulation C, about one-third to that in KOR, and the rest to that in regions other than northeast Asia. By further adding the temporal variation in the domestic (JPN) emissions in simulation E, the increasing trend in the domestic contribution became significant (0.28 ppbv/decade), implying that the increasing trend in domestically produced O_3 was from a combination of multiple factors each of which did not cause a significant increase. The total effect of the emission increase in KOR on the increasing trend in surface O_3 over Japan assessed as the difference between simulations C and D was about 0.38 ppbv/decade; and that of the IAV of domestic emission in Japan assessed as the difference between simulations D and E was about 0.09 ppbv/decade; each of

549 which corresponded to about 16 and 4 % of the increasing trend in total O_3 in the standard
550 simulation, respectively.

551 The IAV in emissions of O_3 precursors in northeast Asian regions (CHN, KOR, and JPN)
552 together with the IAV in the climate and the increase in CH_4 concentration induced a
553 significant increasing trend in total O_3 over Japan with a rate of 1.99 ppbv/decade. This
554 accounted for about 84 % of the increasing trend in total O_3 in the standard simulation. The
555 rest of the increasing trend should be regarded as from O_3 precursor emission changes in
556 regions other than northeast Asia. The difference between simulations E and F (standard
557 simulation) showed that the emission change in such regions influenced surface O_3 over Japan
558 mainly through increasing the O_3 production in WSSE Asia and the FT (Fig. 9).

559

560 ## 4 Summary and conclusion

561 We demonstrated the relative importance of the regions of photochemical O_3 production in
562 the global atmosphere on the long-term increasing trend in surface O_3 over Japan reported in
563 recent decades by conducting a series of tracer-tagging simulations using the global CTM
564 CHASER. The impact of the IAVs of climate, of CH_4 concentration, and of emission of O_3
565 precursors (NO_x and NMVOC) in different source regions on regional photochemical O_3
566 production were also investigated.

567 The observed increasing trend of surface O_3 over Japan for 1980–2005 (2.70 ppbv/decade
568 for annual mean over whole Japan) was successfully reproduced by the model (2.58
569 ppbv/decade) including an obvious tendency of increase toward western Japan and to be
570 greater in the warm (spring–summer) than in the cold season (fall–winter).

571 The absolute contribution of each photochemical O_3 production region to the surface O_3 over
572 Japan represented by the concentrations of tagged O_3 tracer showed different temporal
573 evolution by regions. The contributions of all Asian regions except the northern part (i.e.,
574 CHN, KOR, E-Asia-Seas, JPN, and WSSE) as well as those of the total FT exhibited
575 significant increasing trends during the period. The increasing trend in the contribution of
576 domestically produced O_3 in Japan (i.e., JPN) did not differ much among the different regions
577 in Japan. However, there was a tendency in the increasing trends in contributions of CHN,
578 KOR, and E-Asia-Seas to be large toward western Japan, which was a main cause of the same
579 tendency in the increasing trend in total O_3 and suggested a large impact of intra-regional
580 transboundary air pollution in East Asia.

581 The trends in contributions of most O_3 production regions, except JPN, were larger in the
582 warm than in the cold season, providing a basis for the seasonality in the increasing trend in
583 total O_3 over Japan. Thus, the larger increasing trend of total O_3 in spring than in summer was
584 mainly due to the same tendency in increasing trends in the contributions of northeast Asian
585 regions (CHN, KOR, and JPN), although this was partly compensated by larger increasing
586 trends in the FT and WSSE Asia contributions in summer than spring. In the cold season, the
587 contributions of FT, WSSE Asia, and Remote had larger increasing trends in winter than in
588 fall, which led to a larger increasing trend in total O_3 in winter than in fall.

589 The sum of the trends in contributions of O_3 production regions with sufficient statistical
590 significance accounted for most (about 97 %) of the increasing trend in total O_3 over Japan
591 (2.37 ppbv/decade). The largest portion was attributed to the increasing trend of O_3 produced
592 in CHN (36 %; 0.85 ppbv/decade), followed by that in the total FT (16 %; 0.37 ppbv/decade).
593 The increasing trend in contributions of the other northeast Asian regions (KOR, E-Asia-Seas,
594 and JPN; 0.27–0.34 ppbv/decade) each accounted for about 12–15 % of the total O_3 trend, and

595 the majority of the rest of the total O_3 trend (7 %; 0.16 ppbv/decade) was attributable to
596 WSSE Asia.

597 We further investigated the impact of the temporal variation of controlling factors, such as
598 climate, CH_4 concentration, and emission of O_3 precursors, on photochemical O_3 production
599 in different source regions and its influence on the long-term increasing trend in surface O_3
600 over Japan through a series of sensitivity simulations that gradually added the temporal
601 variation of these factors. The IAV of the climate and the increase in CH_4 concentration
602 together caused the increase of photochemical O_3 production in several regions and resulted
603 in the significant increasing trend in surface O_3 over Japan (0.44 ppbv/decade) and
604 represented about 19 % of the increasing trend in surface O_3 in the standard simulation. The
605 increase in emission of O_3 precursors in CHN led to the increase of photochemical O_3
606 production in northeast Asian regions including CHN itself, KOR, JPN, and E-Asia-Seas; and
607 the resulting increasing trend in surface O_3 over Japan (1.08 ppbv/decade) accounted for
608 about 46 % of that in the standard simulation. The relative contribution of CHN to the surface
609 O_3 increasing trend over Japan as the source region of O_3 precursor "emission" was 10 %
610 larger than as the source region of O_3 "production" due to production of O_3 outside of CHN.
611 Then, the impact of the O_3 precursor emission change in KOR and JPN on the increasing
612 trend in surface O_3 over Japan (about 0.38 and 0.10 ppbv/decade, respectively) corresponded
613 to 16 and 4 % of the increasing trend in total O_3 in the standard simulation, respectively. The
614 rest of the increasing trend in total O_3 in the standard simulation (about 16 %) was attributed
615 to O_3 precursor emission change in regions other than northeast Asia, mainly through
616 increasing the photochemical O_3 production in WSSE Asia and the total FT.

617 The results summarized above depended largely on the forcings of long-term simulation,
618 particularly the long-term variation of the emissions of O_3 precursors in Asia. Zhao et al.
619 (2013) estimated the NO_x emission in China for the period 1995−2010 and compared it to the
620 existing emission inventories including Hao et al. (2002), Zhan et al. (2007), and the version
621 of REAS used in this study. They showed the log-term increasing trend in Chinese NO_x
622 emission in REAS was consistent with that in the other inventories, but the amount of
623 emission was somewhat smaller in REAS than in the others. Therefore, the long-term
624 increasing trend in the contribution of Chinese emission to the surface O_3 over Japan showed
625 in the preset study would be retained if the other emission inventories were used for the
626 simulation but the specific values of the contributions could be affected. Further studies
627 should address the impact these uncertainties in the different emission inventories on the trend
628 of surface O_3 over Japan.

629

630 *Acknowledgements.* This research was supported by the Global Environment Research Fund
631 (S-7) by the Ministry of the Environment (MOE) of Japan and the East Asian Environment
632 Research Program at the National Institute for Environmental Studies (NIES). We
633 acknowledge the entire staff of the EANET and the AEROS air quality monitoring stations of
634 the MOE of Japan and of the local governments for carrying out measurements and providing
635 the observations. The calculations were performed on the NIES supercomputer system (NEC
636 SX-8R, SX9). The GFD-DENNOU library was used for drawing the figures.
637

638 **References**

639 Akimoto, H., Mori, Y., Sasaki, K., Nakanishi, H., Ohizumi, T., and Itano, Y.: Analysis of
640 monitoring data of ground-level ozone in Japan for longterm trend during 1990–2010:
641 Causes of temporal and spatial variation, Atmos. Environ., 102, 302–310, 2015.

642 Akiyoshi, H., Zhou, L. B., Yamashita, Y., Sakamoto, K., Yoshiki, M., Nagashima, T.,
643 Takahashi, T., Kurokawa, J., Takigawa, M., and T. Imamura, T.: A CCM simulation of the
644 breakup of the Antarctic polar vortex in the years 1980–2004 under the CCMVal scenarios,
645 J. Geophys. Res., 114, D03103, doi:10.1029/2007JD009261, 2009.

646 Brasseur, G. P., Schultz, M., Granier, C., Saunois, M., Diehl, T., Botzet, M., and Roeckner,
647 E.: Impact of climate change on the future chemical composition of the global troposphere,
648 J. Clim., 19, 3932–3951, doi:10.1175/JCLI3832.1, 2006.

649 Chang, S.-C. and Lee, C.-T.: Evaluation of the trend of air quality in Taipei, Taiwan from
650 1994 to 2003, Environ. Monit. Assess., 127, 87–96, doi:10.1007/s10661-006-9262-1, 2007.

651 Chou, C. C.-K., Liu, S. C., Lin, C.-Y., Shiu, C.-J., and Chang, K.-H.: The trend of surface
652 ozone in Taipei, Taiwan, and its causes: Implications for ozone control strategies, Atmos.
653 Environ., 40, 3898–3908, 2006.

654 Cooper, O. R., Parrish, D. D., Ziemke, J., Balashov, N. V., Cupeiro, M., Galbally, I. E., Gilge,
655 S., Horowitz, L., Jensen, N. R., Lamarque, J.-F., Naik, V., Oltmans, S. J., Schwab, J.,
656 Shindell, D. T., Thompson, A. M., Thouret, V., Wang, Y., and Zbinden, R. M.: Global
657 distribution and trends of tropospheric ozone: An observation-based review, Elementa, 2,
658 000029, doi: 10.12952/journal.elementa.000029, 2014.

659 Ding, A. J., Wang, T., Thouret, V., Cammas, J.-P., and Nédélec, P.: Tropospheric ozone
660 climatology over Beijing: analysis of aircraft data from the MOZAIC program, Atmos.
661 Chem. Phys., 8, 1–13, 2008.

662 Eyring, V., Harris, N. R P., Rex, M., Shepherd, T. G., Fahey, D. W., Amanatidis, G. T.,
663 Austin, J., Chipperfield, M. P., Dameris, M., Forster, P. M. De F., Gettelman, A., Graf, H.
664 F., Nagashima, T., Newman, P. A., Pawson, S., Prather, M. J., Pyle, J. A., Salawitch, R. J.,
665 Santer, B. D., and Waugh, D. W.: A strategy for process-oriented validation of coupled
666 chemistry-climate models. Bull. Am. Meteorol. Soc., 86, 1117–1133, 2005.

667 Hao, J. M., Tian, H. Z., and Lu, Y. Q.: Emission inventories of NO_x from commercial energy
668 consumption in China, 1995–1998, Environ. Sci. Technol., 36, 552–560,
669 doi:10.1021/Es015601k, 2002.

670 HTAP, UNECE: Hemispheric Transport of Air Pollution 2010: Part A: Ozone and Particulate
671 Matter, Air Pollution Studies No. 17, (ed. by Dentener, F., Keating, T., and Akimoto, H.),
672 ECE/EN.Air/100, 2010.

673 JMA (Japan Meteorological Agency): available online at
674 http://www.data.jma.go.jp/cpdinfo/temp/list/an_jpn.html (In Japanese), 2017.

675 Kalnay, E., Kanamitsu, M., Kistler, R., Collins, W., Deaven, D., Gandin, L., Iredell, M., Saha,
676 S., White, G., Woollen, J., Zhu, Y., Leetmaa, A., Reynolds, B., Chelliah, M., Ebisuzaki,
677 W., Higgins, W., Janowiak, J., Mo, K. C., Ropelewski, C., Wang, J., Jenne, R., and Joseph,
678 D.: The NCEP/NCAR 40-year reanalysis project, Bull. Amer. Meteor. Soc., 77, 437–470,
679 1996.

680 Kawase, H., Nagashima, T., Sudo, K., and Nozawa, T.: Future changes in tropospheric ozone
681 under Representative Concentration Pathways (RCPs), Geophys. Res. Lett., 38, L05801,
682 doi:10.1029/2010GL046402, 2011.

683 Kurokawa, J., Ohara, T., Uno, I., Hayasaki, M., and Tanimoto, H.: Influence of
684 meteorological variability on interannual variations of springtime boundary layer ozone
685 over Japan during 1981–2005, Atmos. Chem. Phys., 9, 6287–6304, 2009.

686 Kurokawa, J., Ohara, T., Morikawa, T., Hanayama, S., Janssens-Maenhout, G., Fukui, T.,
687 Kawashima, K., and Akimoto, H.: Emissions of air pollutants and greenhouse gases over
688 Asian regions during 2000–2008: Regional Emission inventory in ASia (REAS) version 2,
689 Atmos. Chem. Phys., 13, 11019–11058, 2013.

690 Lee, H.-J., Kim, S.-W., Brioude, J., Cooper, O. R., Frost, G. J., Kim, C.-H., Park, R. J.,
691 Trainer, M., and Woo J.-H.: Transport of NOx in East Asia identified by satellite and in
692 situ measurements and Lagrangian particle dispersion model simulations, J. Geophys. Res.
693 Atmos., 119, 2574–2596, doi:10.1002/2013JD021185, 2014.

694 Li, J., Wang, Z. F., Akimoto, H., Yamaji, K., Takigawa, M., Pochanart, P., Liu, Y., Tanimoto,
695 H., and Kanaya, Y.: Near-ground ozone source attributions and outflow in central eastern
696 China during MTX2006, Atmos. Chem. Phys., 8, 7335–7351, 2008.

Li, H. C., Chen, K. S., Huang, C. H., and Wang, H. K.: Meteorologically adjusted long-term trend of ground-level ozone concentrations in Kaohsiung County, southern Taiwan, Atmos. Environ., 44, 3605–3608, 2010.

Lin, S.-J. and Rood, R. B.: Multidimensional flux-form semi-Lagrangian transport scheme, Mon. Weather Rev., 124, 2046–2070, 1996.

Lin, Y.-K., Lin, T.-H., and Chang, S.-C.: The changes in different ozone metrics and their implications following precursor reductions over northern Taiwan from 1994 to 2007, Environ. Monit. Assess., 169, 143–157, 2010.

Logan, J. A., Megretskaia, I. A., Miller, A. J., Tiao, G. C., Choi, D., Zhang, L., Stolarski, R. S., Labow, G. J., Hollandsworth, S. M., Bodeker, G. E., Claude, H., de Muer, D., Kerr, J. B., Tarasick, D. W., Oltmans, S. J., Johnson, B., Schmidlin, F., Staehelin, J., Viatte, P., and Uchino, O.: Trends in the vertical distribution of ozone: A comparison of two analyses of ozonesonde data, J. Geophys. Res., 104, 26373–26399, 1999.

Lu, W.-Z. and Wang, X.-K.: Evolving trend and self-similarity of ozone pollution in central Hong Kong ambient during 1984–2002, Sci. Total Environ., 357, 160–168, 2006.

Mauzerall, D. L., Sultan, B., Kim, N., and Bradford, D. F.: NOx emissions from large point sources: variability in ozone production, resulting health damages and economic costs, Atmos. Environ., 39, 2851–2866, 2005.

Meinshausen, M., Smith. S. J., Calvin, K., Daniel, J. S., Kainuma, M. L. T., Lamarque, J-F., Matsumoto, K., Montzka, S. A., Raper, S. C. B., Riahi, K., Thomson, A., Velders, G. J. M., and van Vuuren, D. P. P.: The RCP greenhouse gas concentrations and their extensions from 1765 to 2300, Climatic Change, 109, 213–241, 2011.

MOE (Ministry of Environment) Japan: FY 2013 status of air pollution, available online at: http://www.env.go.jp/air/osen/jokyoh25/ (in Japanese), 2013.

Nagashima, T., Ohara, T., Sudo, K., and Akimoto, H.: The relative importance of various source regions on East Asian surface ozone, Atmos. Chem. Phys., 10, 11305–11322, 2010.

Naja, M. and Akimoto, H.: Contribution of regional pollution and long-range transport to the Asia-Pacific region: Analysis of long-term ozonesonde data over Japan, J. Geophys. Res., 109, D21306, doi:10.1029/2004JD004687, 2004.

726 Nozawa, T., Nagashima, T., Shiogama, H., and Crooks, S. A.: Detecting natural influence on
727 surface air temperature change in the early twentieth century, Geophys. Res. Lett., 32,
728 L20719, doi:10.1029/2005GL023540, 2005.

729 Ohara, T. and Sakata, T.: Long-term variation of photochemical oxidants over Japan, J. Jpn.
730 Soc. Atmos. Environ., 38, 47–54. (in Japanese with English summary), 2003.

731 Ohara, T., Yamaji, K., Uno, I., Tanimoto, H., Sugata, S., Nagashima, T., Kurokawa, J., Horii,
732 N., and Akimoto, H.: Long-term simulations of surface ozone in East Asia during 1980–
733 2020 with CMAQ and REAS inventory, In Air Pollution Modelling and Its Application
734 XIX (NATO Science for Peace and Security Series C: Environmental Security) (ed. by
735 Borrego, C., and Miranda, A. I.). Springer, Dordrecht, The Netherlands, 136–144, 2008.

736 Ohara, T., Akimoto, H., Kurokawa, J., Horii, N., Yamaji, K., Yan, X., and Hayasaka, T.: An
737 Asian emission inventory of anthropogenic emission sources for the period 1980–2002,
738 Atmos. Chem. Phys., 7, 4410–4444, 2007.

739 Olivier, J. G. J. and Berdowski, J. J. M.: Global emissions sources and sinks, in: The Climate
740 System, Berdowski, J., Guicherit, R., and Heij, B. J. (eds.), A. A. Balkema Publishers/
741 Swets & Zeitlinger Publishers, Lisse, The Netherlands, 33–78, 2001.

742 Oltmans, S. J., Lefohn, A. S., Harris, J. M., Galbally, I., Scheel, H. E., Bodeker, G., Brunke,
743 E., Claude, H., Tarasick, D., Johnson, B. J., Simmonds, P., Shadwick, D., Anlauf, K.,
744 Hayden, K., Schmidlin, F., Fujimoto, T., Akagi, K., Meyer, C., Nichol, S., Davies, J.,
745 Redondas, A., and Cuevas, E.: Long-term changes in tropospheric ozone, Atmos. Environ.,
746 40, 3156–3173, 2006.

747 Oltmans, S. J., Lefohn, A. S., Shadwick, D., Harris, J. M., Scheel, H. E., Galbally, I., Tarasick,
748 D. W., Johnson, B. J., Brunke, E.-G., Claude, H., Zeng, G., Nichol, S., Schmidlin, F.,
749 Davies, J., Cuevas, E., Redondas, A., Naoe, H., Nakano, T., and Kawasato, T.: Recent
750 tropospheric ozone changes – A pattern dominated by slow or no growth, Atmos. Environ.,
751 67, 331–351, 2013.

752 Parrish, D. D., Law, K. S., Staehelin. J., Derwent, R., Cooper, O. R., Tanimoto, H., Volz-
753 Thomas, A., Gilge, S., Scheel, H.-E., Steinbacher, M., and Chan, E.: Long-term changes in
754 lower tropospheric baseline ozone concentrations at northern mid-latitudes, Atmos. Chem.
755 Phys., 12, 11485–11504, 2012.

Rayner, N. A., Parker, D. E., Horton, E. B., Folland, C. K., Alexander, L. V., Rowell, D. P., Kent, E. C., and Kaplan, A.: Global analyses of sea surface temperature, sea ice, and night marine air temperature since the late nineteenth century, J. Geophys. Res., 108, 4407, doi:10.1029/2002JD002670, 2003.

Schultz, M. G., Heil, A., Hoelzemann, J. J., Spessa, A., Thonicke, K., Goldammer, J. G., Held, A. C., Pereira, J. M. C., and van het Bolscher, M.: Global wildland fire emissions from 1960 to 2000, Global Biogeochem. Cycles, 22, GB2002, doi:10.1029/2007GB003031, 2008.

Seo, J., Youn, D., Kim, J. Y., and Lee, H.: Extensive spatiotemporal analyses of surface ozone and related meteorological variables in South Korea for the period 1999–2010, Atmos. Chem. Phys., 14, 6395–6415, 2014.

Shindell, D., Kuylenstierna, J. C. I., Faluvegi, G., Milly, G., Emberson, L., Hicks, K., Vignati, E., Van Dingenen, R., Janssens-Maenhout, G., Raes, F., Pozzoli, L., Amann, M., Klimont, Z., Kupiainen, K., Höglund-Isaksson, L., Anenberg, S. C., Muller, N., Schwartz, J., Streets, D., Ramanathan, V., Oanh, N. T. K., Williams, M., Demkine, V., and Fowler, D.: Simultaneously mitigating near-term climate change and improving human health and food security, Science, 335, 183–189, 2012.

Silva, R. A., West, J. J., Zhang, Y., Anenberg, S. C., Lamarque, J.-F., Shindell, D. T., Collins, W. J., Dalsoren, S., Faluvegi, G., Folberth, G., Horowitz, L. W., Nagashima, T., Naik, V., Rumbold, S., Skeie, F., Sudo, K., Takemura, T., Bergmann, D., Cameron-Smith, P., Cionni, I., Doherty, R. M., Eyring, V., Josse, B., MacKenzie, I. A., Plummer, D., Righi, M., Stevenson, D. S., Strode S., Szopa, S., and Zeng, G.: Global premature mortality due to anthropogenic outdoor air pollution and the contribution of past climate change, Environ. Res. Lett., 8, 034005, 2013.

Sudo, K. and Akimoto, H.: Global source attribution of tropospheric ozone: Long-range transport from various source regions, J. Geophys. Res., 112, D12302, doi:10.1029/2006JD007992, 2007.

Sudo, K., Takahashi, M., Kurokawa, J., and Akimoto, H.: CHASER: A global chemical model of the troposphere: 1. Model description, J. Geophys. Res., 107(D17), 4339, doi:10.1029/2001JD001113, 2002.

786 Susaya, J., Kim, K.-H., Shon, Z.-H., and Brown, R. J. C.: Demonstration of long-term
787 increases in tropospheric O_3 levels: Causes and potential impacts, Chemosphere, 92, 1520–
788 1528, 2013.

789 Tanimoto, H.: Increase in springtime tropospheric ozone at a mountainous site in Japan for
790 the period 1998–2006, Atmos. Environ., 43, 1358–1363, 2009.

791 Tanimoto, H., Ohara, T., and Uno, I.: Asian anthropogenic emissions and decadal trends in
792 springtime tropospheric ozone over Japan: 1998–2007, Geophys. Res. Lett., 36, L23802,
793 doi:10.1029/2009GL041382, 2009.

794 UNEP (United Nations Environment Programme) and WMO (World Meteorological
795 Organization): Integrated Assessment of Black Carbon and Tropospheric Ozone: Summary
796 for Decision Makers, available online at
797 http://www.unep.org/dewa/Portals/67/pdf/Black_Carbon.pdf, 2011.

798 US EPA (U.S. Environmental Protection Agency): Air Quality Criteria for Ozone and Related
799 Photochemical Oxidants (Final), U.S. Environmental Protection Agency, Washington, DC,
800 EPA/600/R-05/004aF-cF, 2006.

801 Van Aardenne, J. A., Dentener, F. J., Olivier, J. G. J., Klein Goldewijk, C. G. M., and
802 Lelieveld, J.: A 1 x 1 degree resolution dataset of historical anthropogenic trace gas
803 emissions for the period 1890–1990, Global Biogeochem. Cy., 15(4), 909–928, 2001.

804 Van Leer, B.: Toward the ultimate conservative difference scheme. IV: A new approach to
805 numerical convection, J. Comput. Phys., 23, 276–299, 1977.

806 Wakamatsu, S., Morikawa, T., and Ito, A.: Air Pollution Trends in Japan between 1970 and
807 2012 and Impact of Urban Air Pollution Countermeasures, Asian J. Atmos. Env., 7(4),
808 177–190, 2013.

809 Wang, X. and Mauzerall, D. L.: Characterizing distributions of surface ozone and its impact
810 on grain production in China, Japan and South Korea: 1990 and 2020, Atmos. Environ., 38,
811 4383–4402, 2004.

812 Wang, T., Wei, X. L., Ding, A. J., Poon, C. N., Lam, K. S., Li, Y. S., Chan, L. Y., and Anson,
813 M.: Increasing surface ozone concentrations in the background atmosphere of Southern
814 China, 1994–2007, Atmos. Chem. Phys., 9, 6217–6227, 2009.

Wang, Y., Zhang, Y., Hao, J., and Luo, M.: Seasonal and spatial variability of surface ozone over China: contributions from background and domestic pollution, Atmos. Chem. Phys., 11, 3511–3525, 2011.

Xu, X., Lin, W., Wang, T., Yan, P., Tang, J., Meng, Z., and Wang, Y.: Long-term trend of surface ozone at a regional background station in eastern China 1991–2006: enhanced variability, Atmos. Chem. Phys., 8, 2595–2607, 2008.

Zhang, Q., Streets, D. G., He, K., Wang, Y., Richter, A., Burrows, J. P., Uno, I., Jang, C. J., Chen, D., Yao, Z., and Lei, Y.: NO_x emission trends for China, 1995–2004: The view from the ground and the view from space, J. Geophys. Res.-Atmos., 112, doi:10.1029/2007jd008684, 2007.

Zhang, Q., Yuan, B., Shao, M., Wang, X., Lu, S., Lu, K., Wang, M., Chen, L., Chang, C.-C., and Liu, S. C.: Variations of ground-level O_3 and its precursors in Beijing in summertime between 2005 and 2011, Atmos. Chem. Phys., 14, 6089–6101, 2014.

Zhao, B., Wang, S. X., Liu, H., Xu, J. Y., Fu, K., Klimont, Z., Hao, J. M., He, K. B., Cofala, J., and Amann M.: NO_x emissions in China: historical trends and future perspectives, Atmos. Chem. Phys., 13, 9869–9897, 2013.

833 **Table 1.** Summary of the linear trends of annual mean tagged O_3 tracers as well as the total O_3
834 averaged over Japan (JPN-ALL) for 1980–2005. Bold figures denote that trends are
835 significant at 5 % risk level.

Source Region	Trend [ppbv/dec]	Percent
CHN	**0.85 ± 0.2**	35.8
KOR	**0.34 ± 0.14**	14.6
JPN	**0.27 ± 0.19**	11.5
E-Asia-Seas	**0.29 ± 0.05**	12.4
WSSE Asia	**0.16 ± 0.04**	6.8
CN Asia	-0.05 ± 0.08	-2.1
Remote	0.04 ± 0.08	1.7
OTH	0.01 ± 0.02	0.5
FT	**0.37 ± 0.1**	15.5
Strat.	0.08 ± 0.28	3.3
Total	**2.37 ± 0.42**	100.0

836
837

838 **Table 2.** Summary of the sensitivity simulations and the standard simulation

Simulation code	CH_4 concentration	O_3 precursor emissions				Stratospheric O_3 trend
		CHN	KOR	JPN	ROW[a]	
A	1980[b]	1980	1980	1980	1980	1980
B	increase[c]	1980	1980	1980	1980	1980
C	increase	Var[d]	1980	1980	1980	1980
D	increase	Var	Var	1980	1980	1980
E	increase	Var	Var	Var	1980	1980
F (standard)	increase	Var	Var	Var	Var	Var

839 a Precursor emissions in the Rest Of the World (ROW) other than CHN, KOR, and JPN

840 b Each factor was fixed at the year 1980 level

841 c CH_4 concentration increased until 2000 and flattened thereafter

842 d Temporal Variation (Var) of each factor was considered

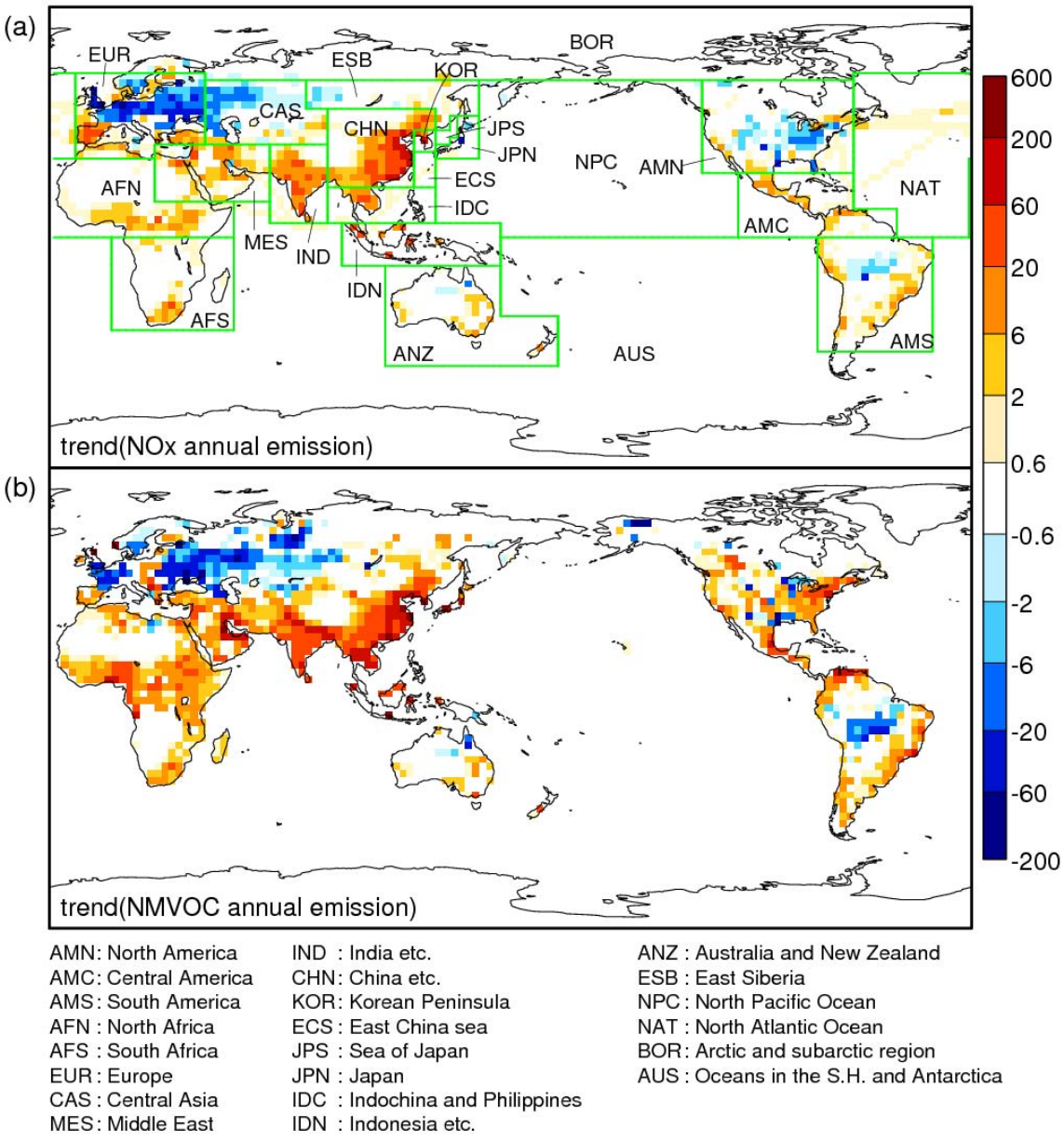

Figure 1. Linear trends of (a) NO_x and (b) NMVOC emission during the simulation period (1980–2005) used in the study. Significant trends at 5 % risk level are colored. Source regions for tracer tagging are also displayed in the top figure.

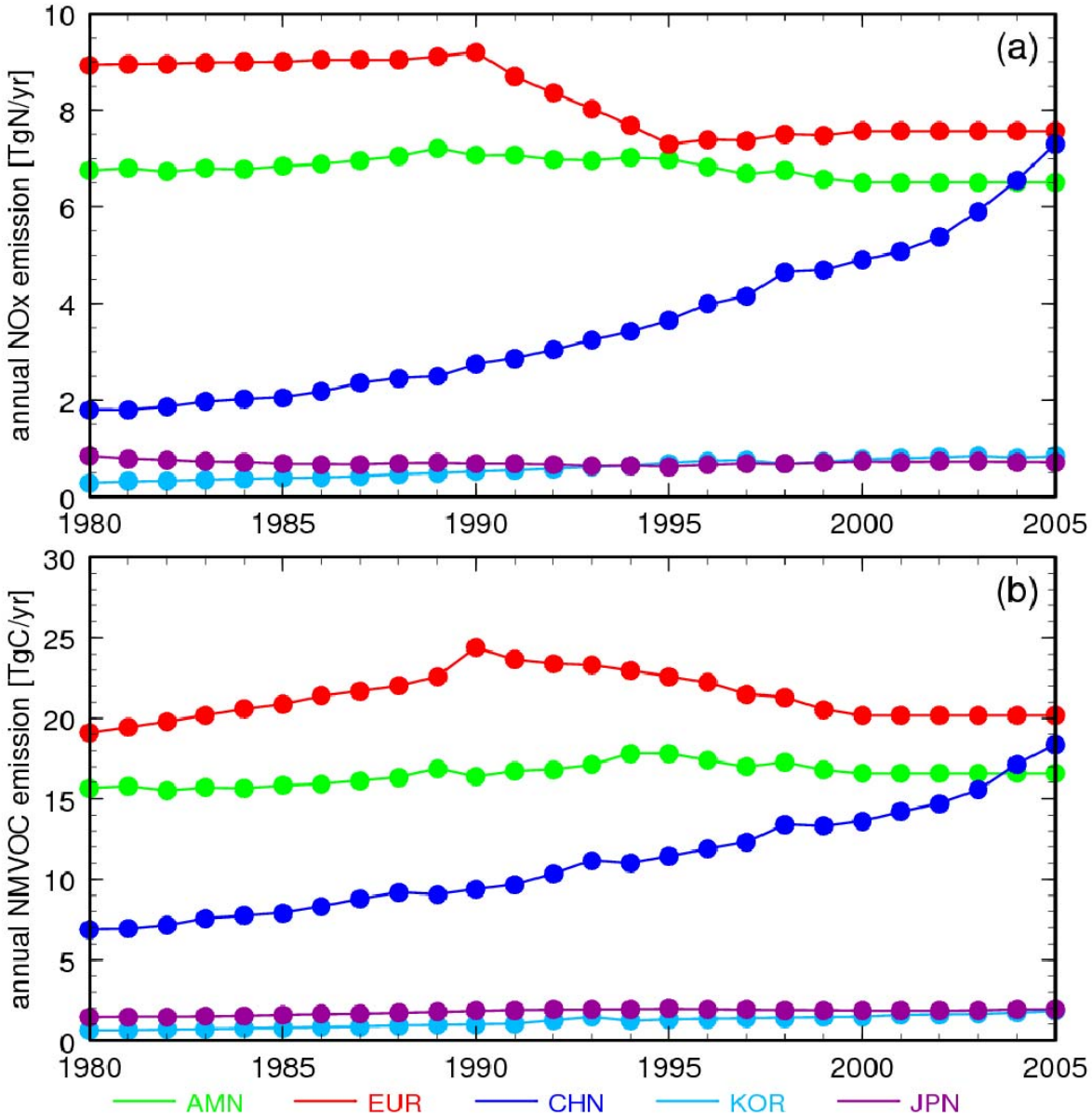

847

848 **Figure 2.** Temporal evolution of emissions of (a) NO_x and (b) NMVOC averaged over several
849 source areas in the Northern Hemisphere depicted in Fig. 1.

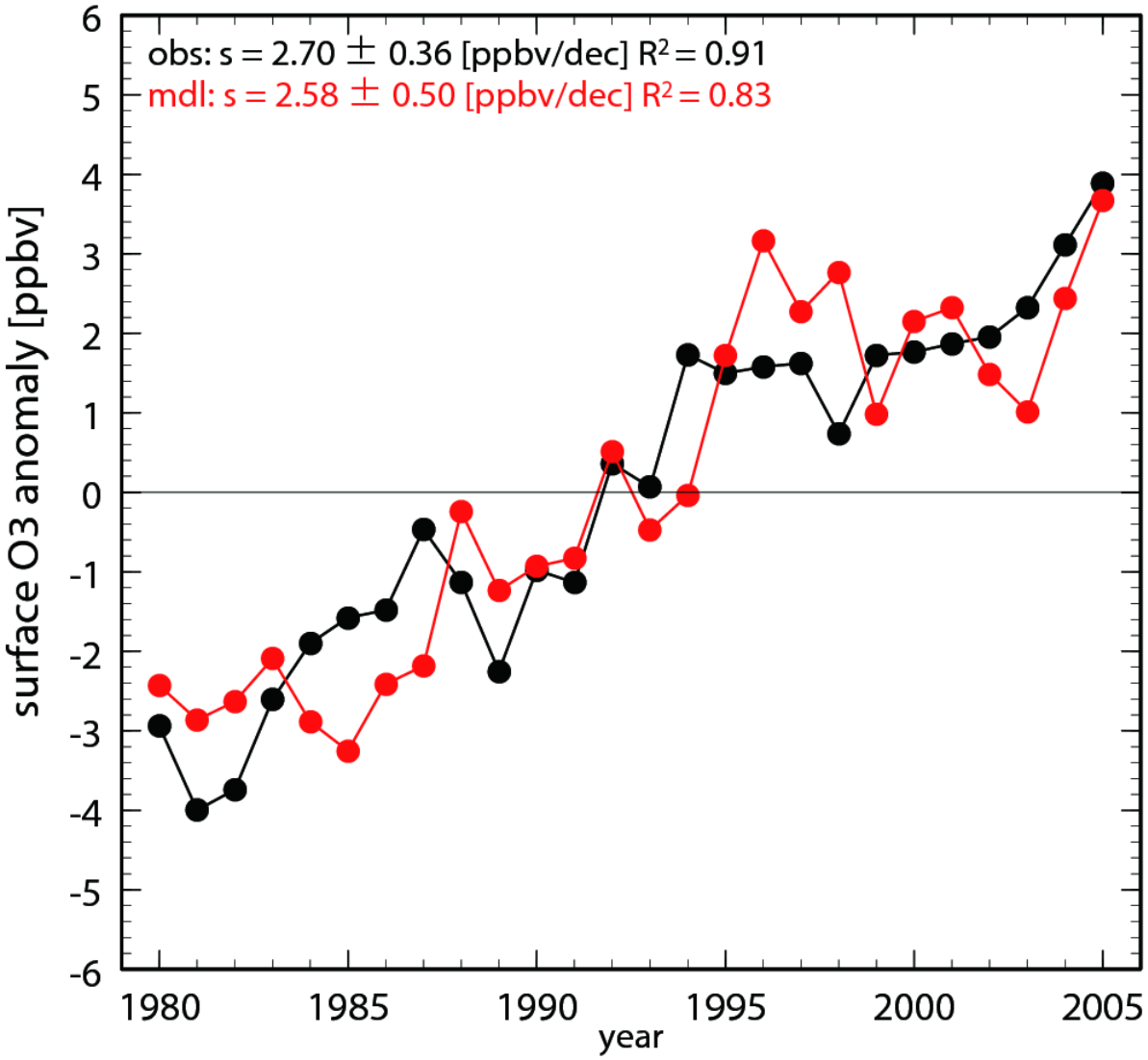

Figure 3. The temporal changes of annual mean surface O_3 anomaly averaged over Japan from observation (AEROS: black) and model calculation (red). Anomalies are defined as deviations from the values averaged over 1980–2005. The slope of a regression (s) for 1980–2005 with their 95 % confidence interval and R^2 are also shown.

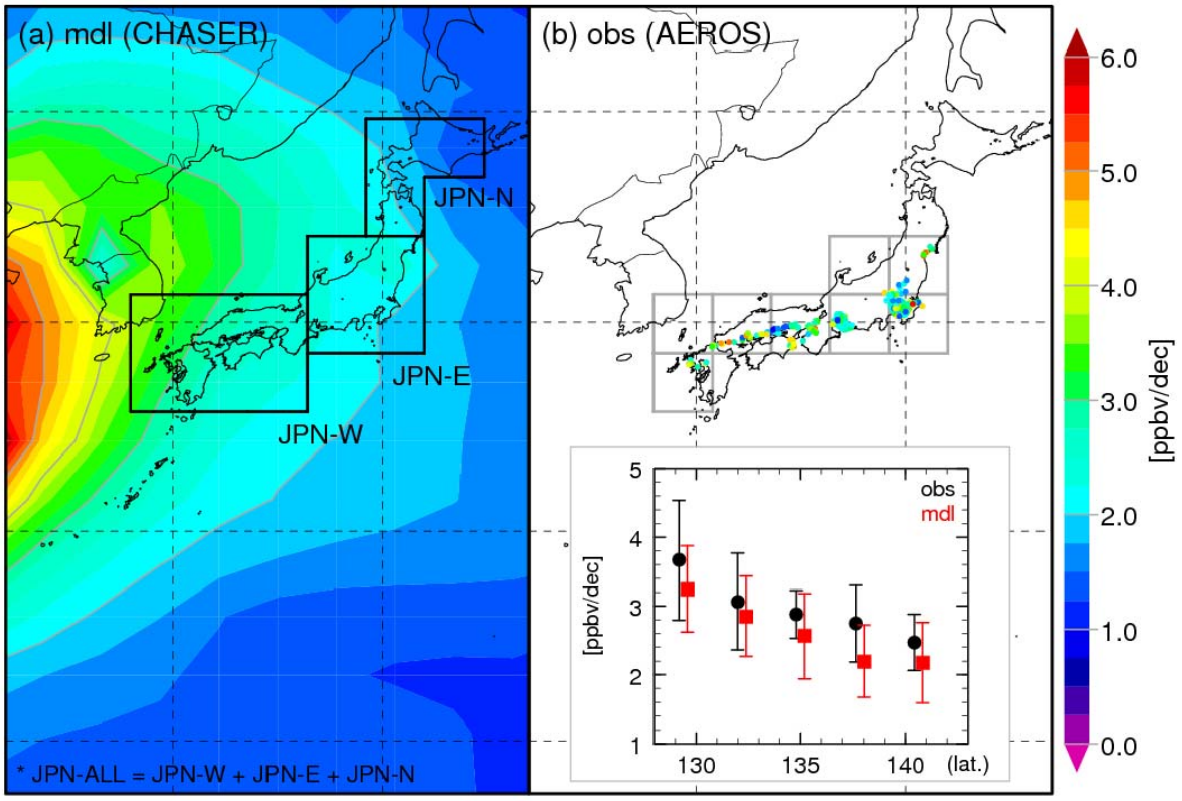

855

856 **Figure 4.** The linear trend of annual mean surface O_3 in 1980–2005 calculated from (a) model
857 simulations and (b) observations at AEROS monitoring sites. The inset in figure (b) shows the
858 longitudinal change of linear trends (black: AEROS observation; red: model) averaged within
859 the model grids shown by gray rectangles. The error bars denote their 95 % confidence
860 intervals. The black-rimmed areas in figure (a) are the area for averaging used in the figures
861 from Fig. 6. Note that JPN-ALL is the sum of JPN-W, JPN-E, and JPN-N areas and used for
862 the averaging in those figures.

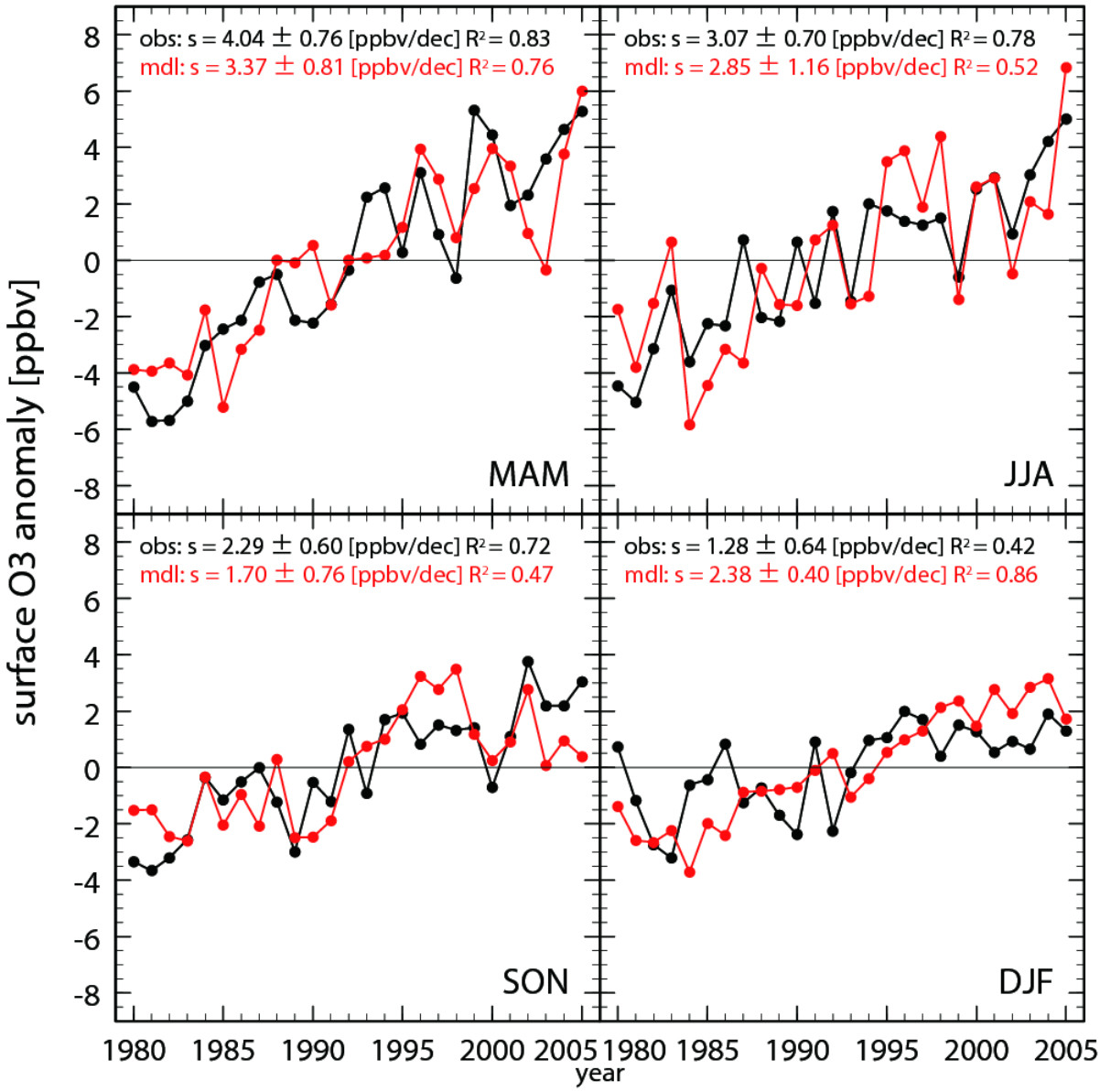

863

864 **Figure 5.** Same as Fig. 3 but the temporal changes of seasonal mean surface O_3 anomaly

865 averaged over Japan from observations (AEROS: black) and model calculations (red).

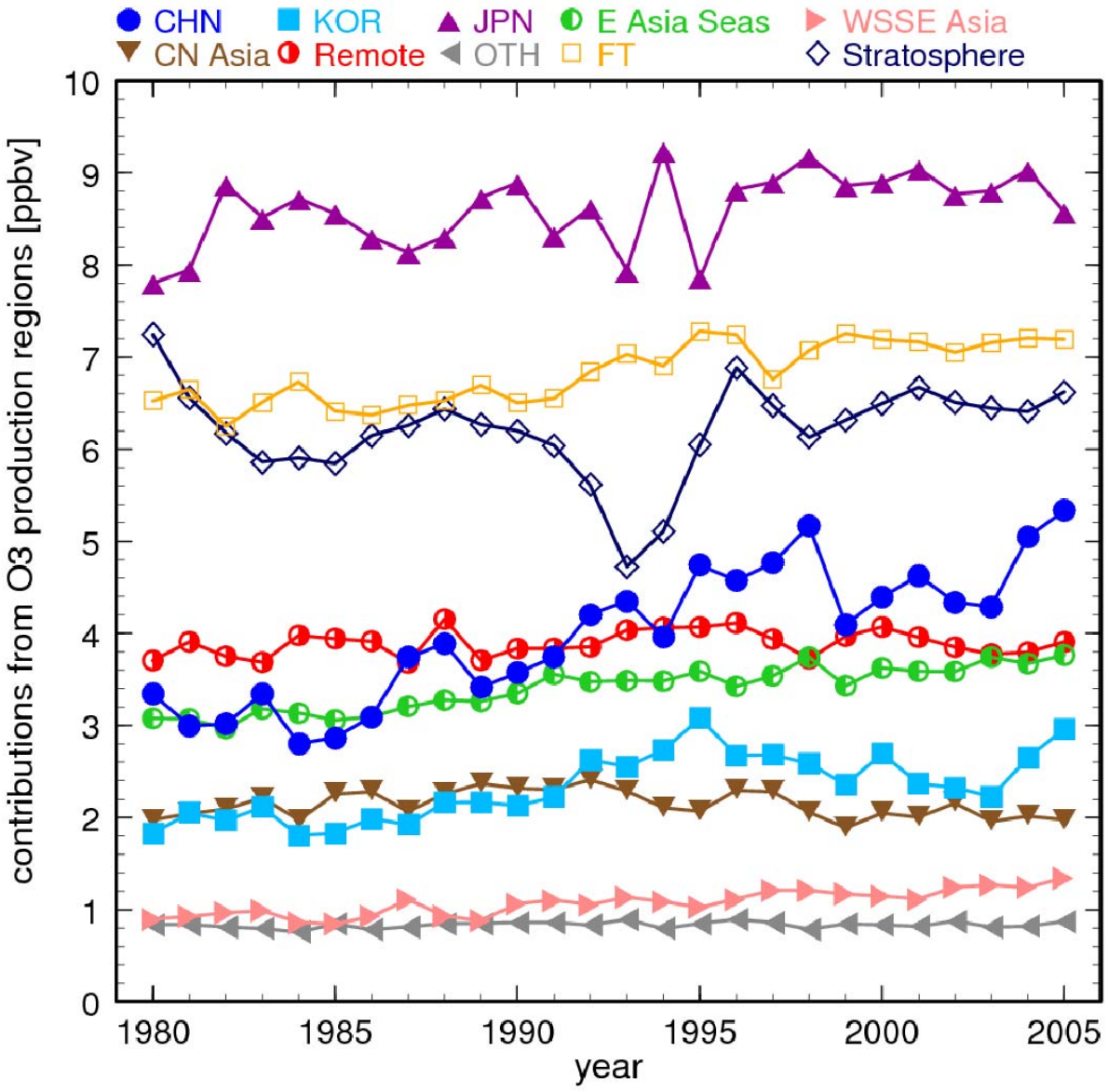

866

867 **Figure 6.** Long-term changes of annual mean contributions from source regions to surface O_3
868 over Japan. Some source regions are grouped: E-Asia-Seas is the sum of NPC, JPS, and ECS;
869 WSSE Asia is the sum of MES, IND, IDN, and IDC; CN Asia is the sum of CAS and ESB;
870 Remote is the sum of AMN, NAT, and EUR; and OTH is the other regions in the planetary
871 boundary layer.

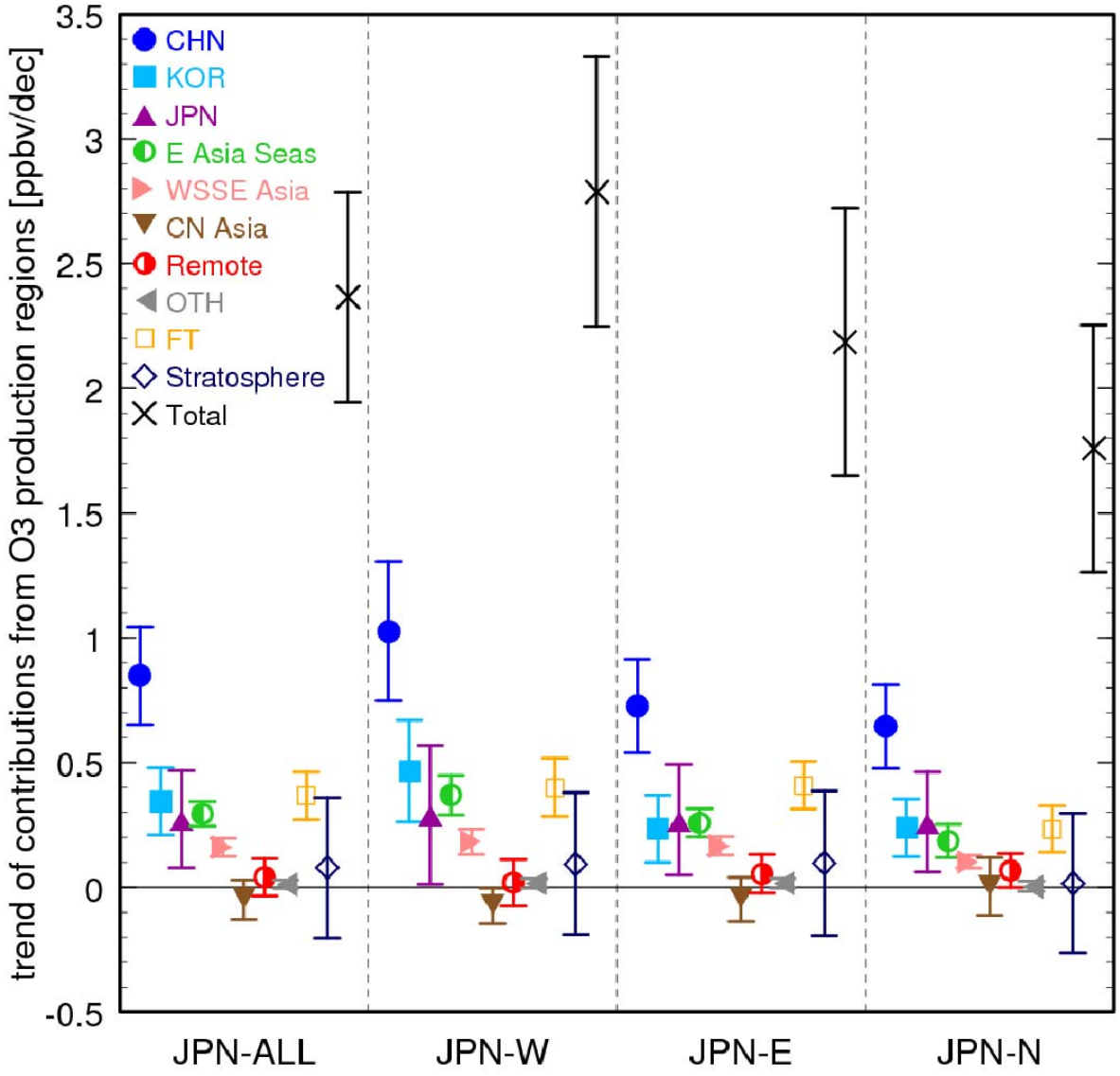

872

873 **Figure 7.** Linear trends of annual mean contributions in 1980–2005 from source regions to
874 surface O_3 over Japan shown in Fig. 6 (JPN-ALL) and those averaged in three sub-regions in
875 Japan (JPN-W, JPN-E, and JPN-N). Error bars are 95 % confidence intervals.

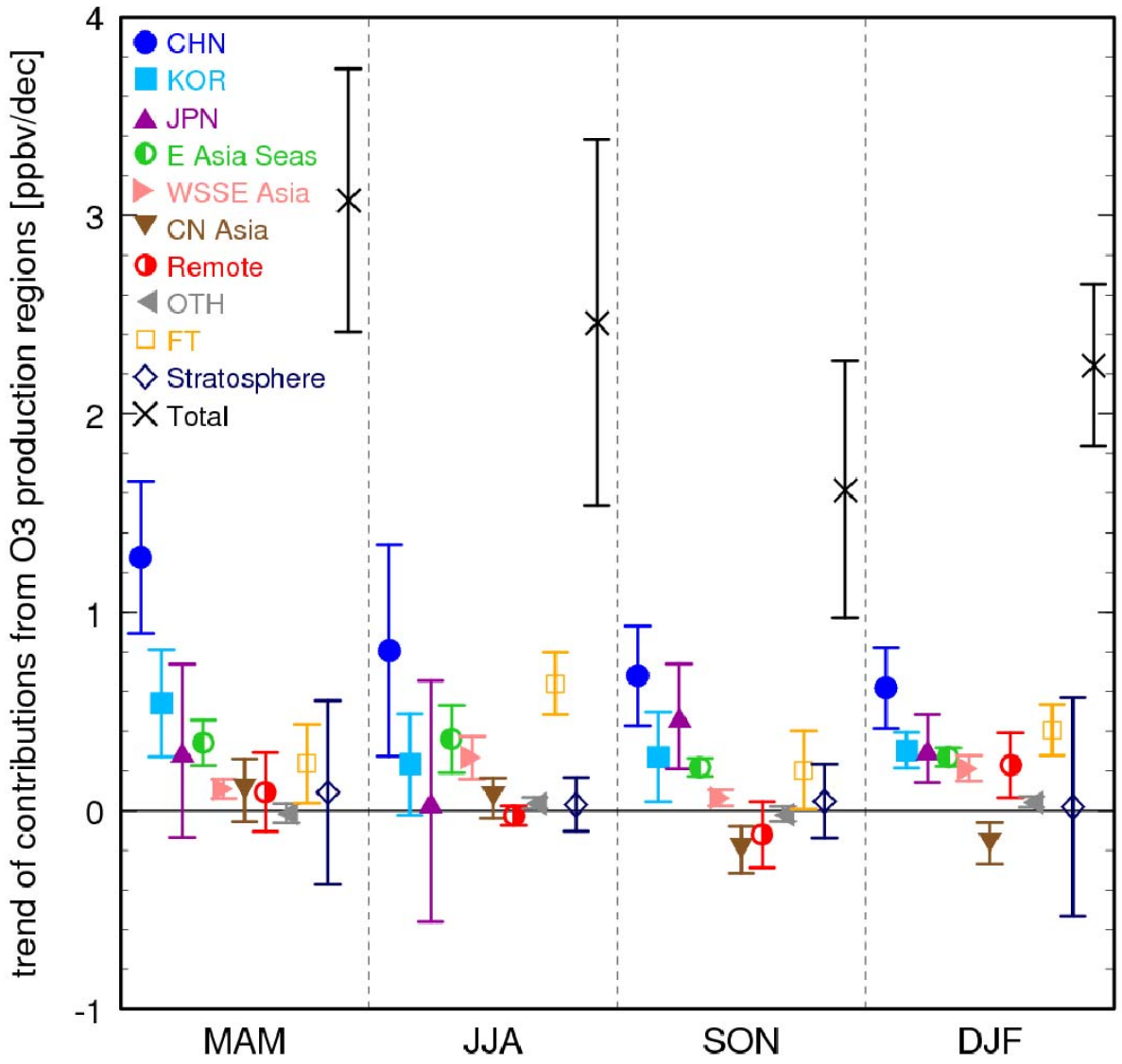

Figure 8. Linear trends of the contributions in 1980–2005 from source regions to surface O_3 over Japan in different seasons: spring (MAM), summer (JJA), fall (SON), and winter (DJF). Error bars are 95 % confidence intervals.

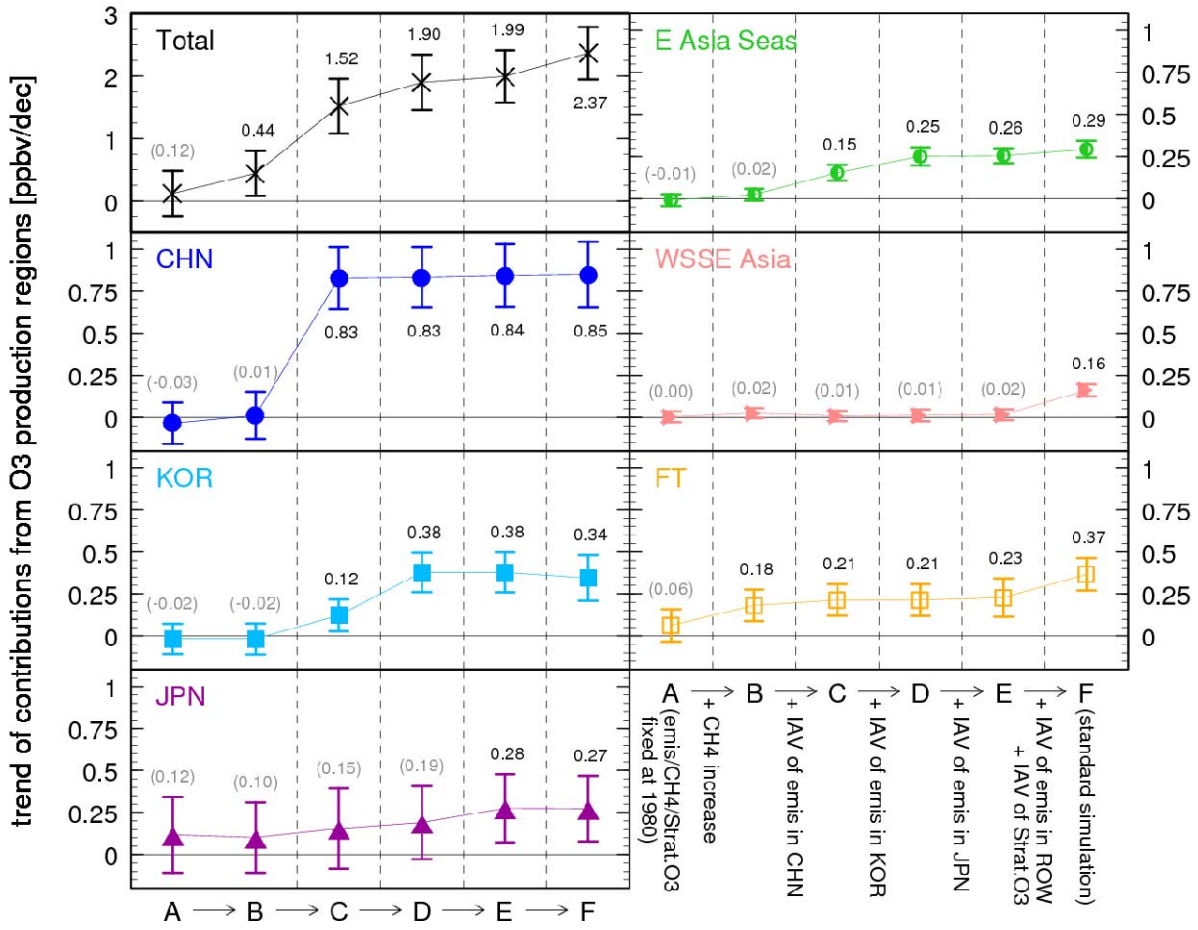

Figure 9. Linear trends of the annual mean contributions in 1980–2005 from source regions to surface O_3 over Japan in the sensitivity simulations and the standard simulation (error bars are 95 % confidence intervals). The exact values of the trends are also shown in the figure; the trends without sufficient statistical significance are shown in parentheses. The trends of each region's contribution in the simulations A–E and F (the standard simulation) are arranged from left to right in each panel.